Made available by Hasselt University Library in https://documentserver.uhasselt.be

Kinetic optimization of multilayered photocatalytic reactors

Peer-reviewed author version

Claes, T; Fransen, S; Degreve, J; Van Gerven, T & LEBLEBICI, Mumin enis (2021) Kinetic optimization of multilayered photocatalytic reactors. In: Chemical engineering journal (1996. Print), 421 (Art N° 127794).

DOI: 10.1016/j.cej.2020.127794
Handle: http://hdl.handle.net/1942/37716

Journal Pre-proofs

Kinetic optimization of multilayered photocatalytic reactors

Thomas Claes, Senne Fransen, Jan Degrève, Tom Van Gerven, M. Enis Leblebici

PII: S1385-8947(20)33914-0
DOI: https://doi.org/10.1016/j.cej.2020.127794
Reference: CEJ 127794

To appear in: *Chemical Engineering Journal*

Received Date: 1 September 2020
Revised Date: 30 October 2020
Accepted Date: 16 November 2020

Please cite this article as: T. Claes, S. Fransen, J. Degrève, T. Van Gerven, M. Enis Leblebici, Kinetic optimization of multilayered photocatalytic reactors, *Chemical Engineering Journal* (2020), doi: https://doi.org/10.1016/j.cej.2020.127794

This is a PDF file of an article that has undergone enhancements after acceptance, such as the addition of a cover page and metadata, and formatting for readability, but it is not yet the definitive version of record. This version will undergo additional copyediting, typesetting and review before it is published in its final form, but we are providing this version to give early visibility of the article. Please note that, during the production process, errors may be discovered which could affect the content, and all legal disclaimers that apply to the journal pertain.

© 2020 Published by Elsevier B.V.

Kinetic optimization of multilayered photocatalytic reactors.

Thomas Claes[a], Senne Fransen[a], Jan Degrève[a], Tom Van Gerven[a], M. Enis Leblebici[b*]

[a]KU Leuven, Department of Chemical Engineering, Celestijnenlaan 200F, B-3001 Heverlee, Belgium

[b]KU Leuven, Center for Industrial Process Technology, Department of Chemical Engineering, Agoralaan Building B, 3590 Diepenbeek, Belgium

thomas.claes@kuleuven.be

senne.fransen@kuleuven.be

tom.vangerven@kuleuven.be

jan.degreve@kuleuven.be

[*]Corresponding author. Email address: muminenis.leblebici@kuleuven.be

ABSTRACT

Translucent structured reactors have proven to be an effective design to scale up microreactors. By generating surface area, this flexible reactor design allows to increase the catalyst loading without increasing the catalyst layer thickness, which is beneficial in tackling diffusion limitations in single-channel reactors. However, adding more depth to such a structure by replicating the channels increases the number of scattering boundaries which leads to energy losses. As a result, there is a design problem which seeks to define the optimal catalyst layer thickness and optimal number of repeating boundaries on a light path. Most of the models are numerically solved and very specific to the reactor type being modeled. In this work, a catalyst layer mass balance model is used to construct a model of a translucent structured reactor which takes into account internal mass transfer

Journal Pre-proofs

effects and which can be used to design an optimal structure. The model is simplified to obtain a graphical tool and an analytical model which is validated to estimate the overall reactor kinetics as a function of dimensionless groups. For a conventional range of parameters, the optimal catalyst layer thickness and optimal number of structural layers was equal to 2 μm and 4, respectively. The presented tools in this work are a step forward in the fabrication of design methods for photocatalytic reactor structures. This way, the designer can easily estimate the design outcome without any complex calculations.

Key words: Photocatalysis, structured reactors, kinetic optimization, design correlations, Graphical tool, dimensionless numbers

1 Introduction

In photocatalytic reactor design, an optimal synergy between photon transport, mass transport, and catalyst loading is desired. Achieving optimal design requires methods to address this parameter space and find the most favorable operating window.

In the past decades several proof-of-concept photoreactor designs were introduced. A typical photocatalytic reactor consists of an illuminated reactor vessel, where the catalyst is either present as individual particles in a slurry or immobilized on a surface. Although easy to use, slurry reactors are not preferred because a particle separation step is required after the reactor. Additionally, the particles can cause clogging when being used in flow [1]. For reactors where the catalyst is immobilized, the catalyst loading increases when thicker layers are deposited on a suitable substrate. Ideally, the layer is sufficiently thick to absorb all the incident light. For example, for TiO_2, a widely used and cheap photocatalyst, the cutoff thickness is approximately equal to 10 μm [2]. A promising reactor design is the microreactor. Microreactors are tackling mass transfer,

photon transfer, and catalyst loading problems simultaneously. Mass and photon transfer limitations are overcome by thin coating layers while the relative catalyst load is high due to a large specific surface area (5000 m^{-1} to 250 000 m^{-1}) [3]. Although microreactors are very productive with respect to their reacting volume, their flow rate is low (~μL min^{-1}) and not all incoming light energy can be captured. This issue is dealt with by incorporating multiple microchannels into a translucent structure. Monoliths, packed beds, 3D printed structures or foams are examples of possible catalyst supports to increase the total surface area and productivity in comparison with microreactors [4–10]. More recently, a microstructured packed bed reactor was developed which could achieve microreactor kinetics ($k_{app} \approx 0.8\ min^{-1}$) while possessing a high productivity [11].

Translucent structures in photoreactor design show potential but the experimental nature of some studies mentioned above do not allow for a prediction of the kinetics of a particular design. In this study, firstly, the most important design parameters of a translucent structure are identified. For a photocatalytic structure illuminated perpendicular to the flow, the structural channel number and the catalyst layer thickness are determining. The structural channel number describes the structure as a number of stacked individual channels and determines the total surface area. The catalyst layer thickness, together with the surface area, determines the catalyst loading. Increasing the catalyst layer thickness increases the amount of light energy being absorbed in the reactor but will lead to diffusion limitations when the layer thickness becomes too large. Increasing the incident light energy has a similar effect. Diffusion limitations are tackled by decreasing the layer thickness which decreases the catalyst loading. Applying thinner catalyst layers while keeping the catalyst loading constant can only be done by increasing the external surface area. As a result, the number of structural channels is required to increase, leading to a larger number of scattering boundaries, resulting in larger light attenuation and energy loss due to scattering. Consequently, a single-

channel reactor absorbs more light energy than a multi-channel reactor with equal catalyst loading. Hence, there is a trade-off between surface area creation and layer thickness reduction. A substantial number of experiments would be required to tackle this optimization problem. Therefore, it is necessary to construct a model which helps to design a multi-channel reactor.

A photoreactor model requires a description of light and mass transport. Light transport is usually modeled by the radiative transfer equation, which describes the absorption and scattering of light in the investigated medium while mass transfer is described by the convection-diffusion equation [12–15]. The radiative transfer equation can only be solved numerically. Some simplifications exist such as the two-flux model (TFM) and six-flux model (SFM). Li Puma et al. [16] and Brucato et al. [17] compared the behavior of the SFM, TFM, and the Lambert-Beer law for a continuous slurry reactor with Monte Carlo solution of the radiative transfer equation. They concluded that both the SFM and TFM are good approximations to the Monte Carlo solution, which demonstrates that simplifications are promising for simplifying energy propagation analysis of photocatalytic reactors. For immobilized reactors, a discrete model rather than a continuous model is required because the photon flux changes at very specific locations in the reactor while it stays constant in between those locations. A promising strategy is the radiation model developed by Imoberdorf et al. [18] which is based on the laws of geometrical optics in which the boundaries of the structure are described separately.

For a heterogeneous photocatalytic model, if the reagents do not absorb light, the light intensity is decoupled from the concentration of the reagents. Hence, the obtained light intensity flux is directly inserted in the mass balance as the rate of energy absorption is assumed to be independent from the conversion. For the convection-diffusion-reaction equation, a distinction is made between the catalyst domain (the light absorbing domain) and the fluid domain. Khodadian et al. [19,20]

modeled a TiO_2 coated annular reactor. They assumed that all the emitted light energy was absorbed by the catalyst due to the reflectivity of the reactor. This simplifies the model since no equation is needed for the light absorption in the catalyst layer. Leblebici et al. [14] modeled a flat plate reactor using computational fluid dynamics together with the convection-diffusion equation to model the reactor behavior. Yet, the light penetration in the catalyst domain was approximated by a linear profile. Visan et al. [12] modeled a microreactor and represented the photocatalytic reaction as a surface reaction with a rate constant depending on the internal diffusion and light absorption profile in the catalyst layer. A similar approach was used by Nielsen et al. [15].

The examples above focus on numerical solutions for the mass balance equations of a photocatalytic reactor. Obtaining the overall kinetics as a function of the number of layers and the catalyst layer thickness via graphical tools or analytical expressions is useful in the designing process. Padoin et al. [2] made an effort in constructing an equation to directly calculate the optimal layer thickness for a single-channel photocatalytic reactor. However, these design equations are based on numerical simulations and are only valid for single-channeled reactors.

Here, we developed an analytical model based on the analytical solution of the reaction-diffusion equation in the catalyst, which researchers can use to design structured photocatalytic reactors. In addition, a graphical tool is presented which can be used to determine reaction rates as a function of dimensionless parameters for single-channel and multi-channel reactors. The model is able to predict the kinetic performance of a single-channel reactor as a function of physical parameters including the optical properties and structural parameters like the catalyst layer thickness and number of structural layers. The model is built on the simplification of a reactor structure into different structural channels where mass transfer from the bulk liquid to the surface can be neglected.

First, the simplifications of the geometry are discussed. Secondly, the model equations are presented as well as the analytical solution. Thirdly, the numerical solution is compared with the analytical solution justifying the assumptions. The simplified model is then validated via literature data from Vezzoli et al. [21]. To conclude, the strategy of finding an optimal reactor configuration for multi-channel reactors is discussed.

2 Theory

2.1 Translating the packed bed structure into an equivalent series of layers

The aim of this work is to assess the combined molar flux through different photocatalytic layers rather than the molar flux through a single catalyst layer. Therefore, the two important design parameters are the catalyst layer thickness and the number of structural layers. Structural channels can be defined as the space in between the structural layers. Due to the complexity of the catalytic reactor structure, simplifications are required for evaluating the molar flux. Throughout the work, different assumptions are made resulting in different solutions of the problem. Figure 1 can be used as a guideline throughout the coming parts. In Figure 2, a schematic of a packed bed structure (A) and its simplified representation (B) are shown. The reactor presented in Figure 2A is a cross-current illuminated packed bed reactor meaning light enters from one side perpendicular to the flow. On the left side of Figure 2B, it is shown that the structure can be translated to a series of layers which are coated on both sides. For every structure, the number of structural layers (n) can be determined, which is based on the number of boundaries a photon passes on its path through the reactor and on the number of channels in the cross-sectional area. Both sides of each layer are exposed to light due to scattering from the other layers. Hence, every layer is front-side illuminated (FSI) and back-side illuminated (BSI). For FSI, photon flux and molar flux have the same direction and are defined at the same boundary. For BSI, the photon flux and molar flux have opposite

directions and are defined at opposite boundaries. I_f (W m^{-2}) is the forward photon flux in the structure and I_b (W m^{-2}) is the backward-scattered photon flux in the structure. Both fluxes can irradiate a catalyst layer front-sided or back-sided, depending on the position of the catalyst layer in the structure. The equation to determine the local volumetric rate of photon absorption in a single catalyst layer is based on the Lambert-Beer law [15].

$$E_a(y) = I_{\mathrm{FSI}}\beta e^{-\beta y} + I_{\mathrm{BSI}}\beta e^{-\beta\delta}e^{\beta y} \quad (1)$$

Where E_a(W m^{-3}) is the local rate of energy absorption, I_{FSI}(W m^{-2}) is the front-side incoming light flux, I_{BSI}(W m^{-2}) is the back-side incoming light flux, β (m^{-1}) is the absorption coefficient, δ (m) is the catalyst layer thickness, and y (m) is the spatial coordinate. To obtain E_a, this equation requires the calculation of all the relevant photon fluxes in the complex structure using a numerical light model. This equation is used for the full numerical calculation of the problem as indicated in Figure 1. Here, we will simplify the equation assuming front-side illumination only since it is used in the solution of the mass balance later on. This is a valid assumption when the concentration profile and energy absorption profile in the catalyst layer are not very steep, which is assessed and confirmed later. As a result, the light flux $I_f^{(2)}$ that hits the catalyst layer from the back side (see left side Figure 2B) is assumed to be coming from the front side as indicated on the right side of Figure 2B. The local volumetric rate of photon absorption is calculated using the first term of Eq. **Error! Reference source not found.**:

$$E_a(y) = I_{\mathrm{FSI}}\beta e^{-\beta y} \quad (2)$$

Within a structure, I_{FSI} is unknown and needs to be modeled, or estimated. On the right side of Figure 2B, it is shown that one structural layer, which is coated with catalyst on both sides, is split in two separate boundaries. As mentioned, the light flux and reagents are provided from the same

side. The convenient choice for the light flux is the forward flux, since this is the highest flux. The first and easiest approach to estimate the forward flux without the use of a model is to ignore scattering and only use the measured absorption coefficient to define the exponential decaying light intensity profile. The second strategy is to fit experimental transmission measurements to an exponential function and subsequently estimate the forward flux. Here we use scattering for the calculation of the forward flux, but do not consider the backward light flux which is the result of backscattering. The validity of this assumption depends on the optical density of the layers. In Figure 3, the ratio between the estimated absorbed energy (E_f), taking into account the assumptions made above, and the numerically calculated absorbed energy ($E_{\max}$), taking into account forward and backward photon flux, is presented as a function of the number of structural layers n for a boundary reflection coefficient equal to 0.075. The details about the model used to calculate $E_{\max}$ as well as the significance of the reflection coefficient is explained thoroughly in earlier work [22]. Since the light model is one-dimensional, light is assumed to be collimated. The scattering of light energy inside the real structure is accounted for using the reflection coefficient. Although the number of layers is a discrete number, it is plotted continuously in Figure 3 to show trends. Not including scattering overestimates the absorbed energy while taking scattering into account underestimates the absorbed energy. It is expected that the error for these assumptions is the highest for a large number of low optical density layers because scattering becomes important when the optical density is low and the number of layers high. The resulting error on the kinetic prediction is dependent on the optimal layer thickness and the number of layers and is discussed in the results section.

Journal Pre-proofs

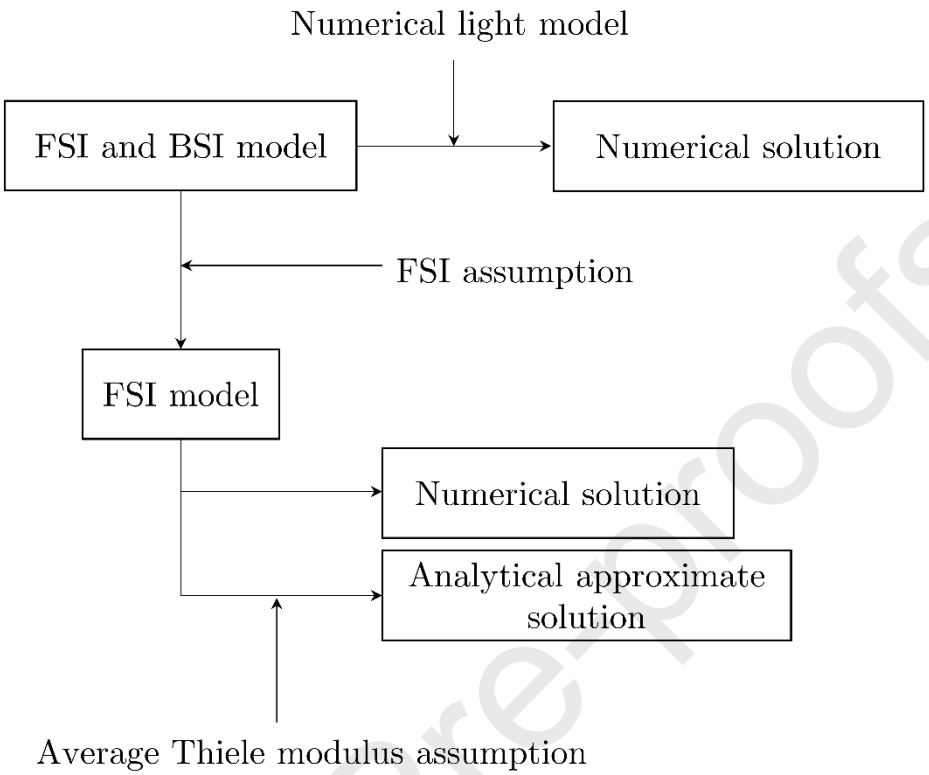

Figure 1: Schematic of the different model solutions and assumptions used in this work.

Journal Pre-proofs

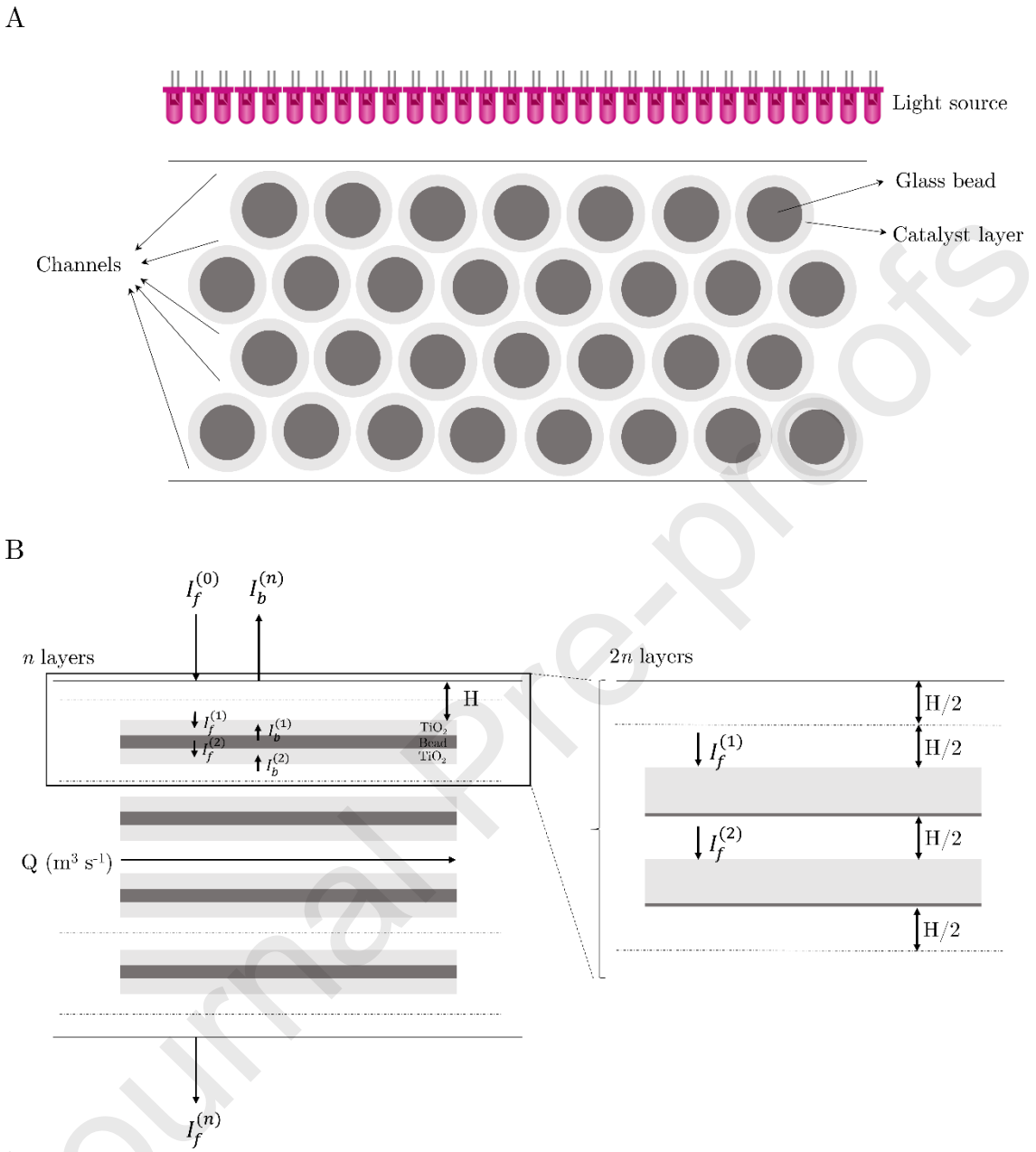

Figure 2: Simplification of a translucent photocatalytic structure to a series of surfaces. The top image presents a scheme of a cross-current illuminated packed bed reactor. The bottom image shows the simplified version of the structured reactor. Q ($m^3 s^{-1}$) is the volumetric flow rate, and H (m) the channel height. The translation of one layer of beads to one plate is regarded as a structural layer and is indicated by the rectangle on the left side of figure B. Dark grey is used for representing the glass bead while light grey is used to represent the catalyst layer.

Journal Pre-proofs

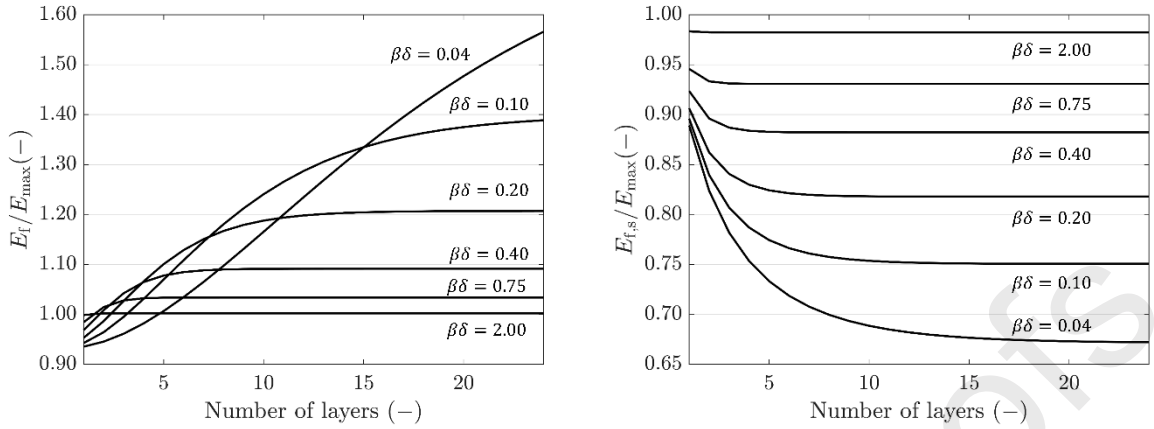

Figure 3: Ratio of the estimated absorbed energy (E_f) to the actual absorbed energy (E_{max}) considering forward flux without scattering (left) and with scattering (right) for a different number of layers and different values of $\beta\delta$.

2.2 Mass transport and chemical reaction inside a catalytic layer

As mentioned, the structure consists of a number of catalyst layers. First, the analysis of a single catalyst layer is made. This is a single porous catalyst coating as presented in Figure 4, where reagents are provided from one side, and light energy enters from both sides.

Journal Pre-proofs

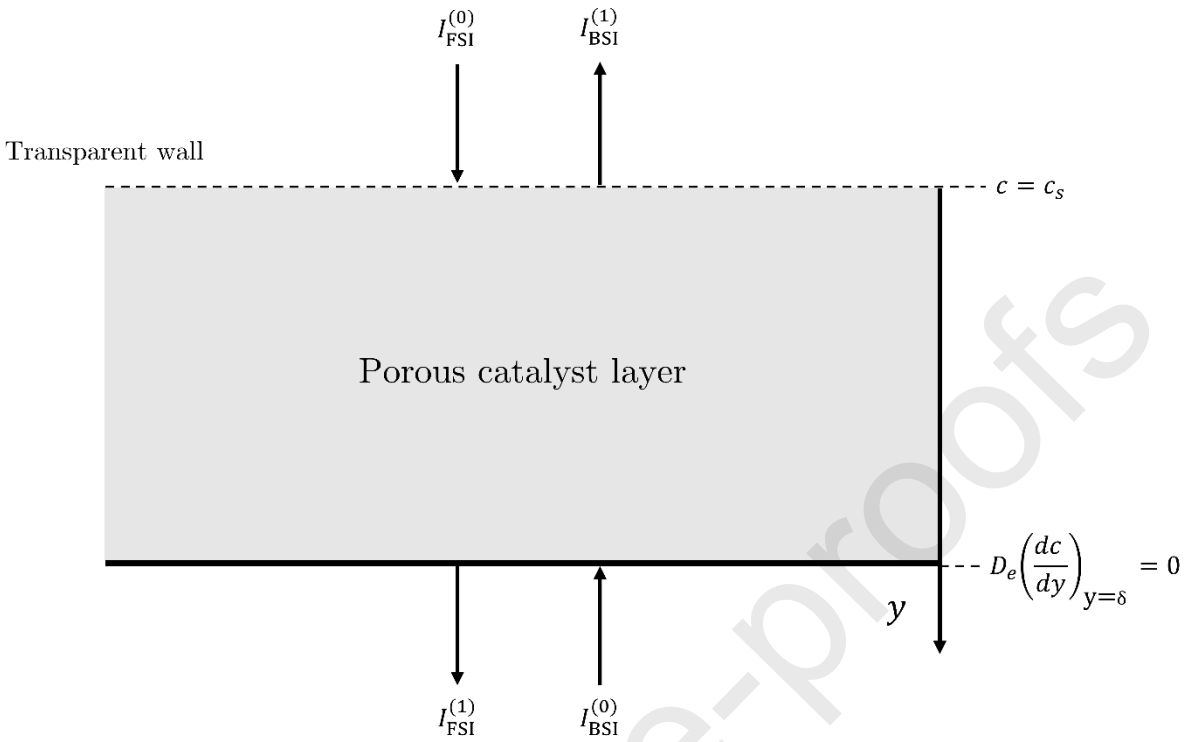

Figure 4: Visualization of a porous catalyst layer irradiated from two sides where $I_{FSI}^{(0)}$ (W m^{-2}) is the incoming light intensity from the front side, $I_{FSI}^{(1)}$ (W m^{-2}) the transmitted light intensity at the back side, $I_{BSI}^{(0)}$ (W m^{-2}) the incoming light intensity from the back side and $I_{BSI}^{(1)}$ (W m^{-2}) the transmitted light intensity at the front, c_s (mol m^{-3}) is the species concentration at the catalyst surface, and $D_e\frac{dc}{dy} = 0$ is the zero flux boundary condition at the layer inner part.

Assume that the reaction is first-order in terms of concentration, which is plausible when the reagent concentration is lower than 1 mM [23]. The mass balance over the catalyst layer for a first-order reaction can be written as

$$D_e\frac{d^2c}{dy^2} - k_i c = 0 \qquad 3$$

Here, D_e(m^{2}s^{-1}) is the effective diffusivity, c (mol m^{-3}) is the species concentration, y (m) is the spatial coordinate, and k_i (s^{-1}) is the intrinsic first-order rate constant. If we take $\tilde{c} = c/c_s$ and $\tilde{y} = y/\delta$, where δ (m) is the layer thickness, the equation can be written in dimensionless form:

$$\frac{d^2\tilde{c}}{d\tilde{y}^2} - \phi^2\tilde{c} = 0 \qquad 4$$

Journal Pre-proofs

The square root of the dimensionless parameter in the reaction term is known as the Thiele modulus:

$$\phi = \delta\sqrt{\frac{k_i}{D_e}} \qquad 5$$

The Thiele modulus relates reactivity to diffusive mass transport in the layer. For first-order reactions, the Thiele modulus is independent of the spatial coordinate. The solution of Eq. **Error! Reference source not found.** is well known and can be found in engineering textbooks [24]. The molar flux is given by

$$N = D_e\frac{dc}{dy} = \frac{D_e c_s d\tilde{c}}{\delta\ d\tilde{y}} = \frac{D_e c_s}{\delta}\tilde{N} = \frac{D_e c_s}{\delta}\phi\tanh(\phi), \qquad 6$$

where N is the molar flux through the catalyst surface, $\tilde{N}$ is the dimensionless molar flux, and ϕ is the Thiele modulus. However, in photocatalysis, the intrinsic rate constant is dependent on the absorbed light energy, which depends on the spatial coordinate inside the catalyst layer. Assuming the rate constant is a function of the absorbed energy rate to the power of a particular constant α_2, the intrinsic rate constant is equal to [12,15]:

$$k_i = \alpha_1 {E_a}^{\alpha_2} \qquad 7$$

Where α_1 is an empirically fitted constant which is dependent on the catalyst and chemical system, α_2 is the power law exponent usually having a value between 0.5 and 1, which is related to the electron-hole recombination rate, and $E_a(\mathrm{W\ m^{-3}})$ is the rate of energy absorption determined by Eq. **Error! Reference source not found.** and Eq. **Error! Reference source not found.**. The mass balance over 1 catalyst layer (see Eq. **Error! Reference source not found.**) then becomes

$$\frac{d^2\tilde{c}}{d\tilde{y}^2} - \frac{\alpha_1\delta^2}{D_e}(I_{\mathrm{FSI}}\beta e^{-\beta\delta\tilde{y}} + I_{\mathrm{BSI}}\beta e^{-\beta\delta}e^{\beta\delta\tilde{y}})^{\alpha_2}\tilde{c} = 0 \quad (8)$$

This equation takes into account FSI as well as BSI. This equation is only numerically solvable. In this work, all the numerical solutions are obtained using a finite difference method using a second-order central difference scheme. In addition, it requires the forward photon flux and backward photon flux, which is calculated taking into account scattering phenomena. This also requires a numerical model. The solution of this equation will be used further in this work as a benchmark to assess the approximate analytical derivation (also see Figure 1).

2.3 Analytical derivation

Eq. **Error! Reference source not found.** can only be solved analytically when the reaction term is reduced to a single photon flux. Here, only FSI is assumed for the analytical derivation because the first catalyst layer, which has the highest incident light intensity, is always front-side illuminated. The reduced Eq. **Error! Reference source not found.** is equal to:

$$\frac{d^2\tilde{c}}{d\tilde{y}^2} - \phi_0^2 e^{-B\tilde{y}}\tilde{c} = 0 \quad (9)$$

Where two dimensionless groups can be distinguished:

$$\phi_0^2 = \frac{\alpha_1\delta^2(I_0\beta)^{\alpha_2}}{D_e} \quad (10)$$

$$B = \alpha_2\beta\delta \quad (11)$$

Where ϕ_0^2 is the squared maximum Thiele modulus at $\tilde{y} = 0$, while B is the optical density of the layer, modified with the recombination fitting parameter α_2 determining the absorption profile over the catalytic layer. B is primarily defined by the optical density $\beta\delta$ because α_2 is a fixed empirical constant fitted together with α_1. For example, when the absorption coefficient increases, light is

Journal Pre-proofs

absorbed at a higher rate and the light flux will decay faster, resulting in a steeper energy absorption profile.

The mass balance over the catalyst layer shows that the reactivity of the catalyst layer changes according to the exponential light intensity decay. As a result, the intrinsic rate constant varies as a function of the spatial coordinate. This also means that the Thiele modulus, which is normally a constant throughout the layer, now varies.

$$\phi^2(\tilde{y}) = \phi_0^2 e^{-B\tilde{y}} \qquad 12$$

The dependency of the reactivity on the spatial coordinate complicates the solution of this equation. Although it is still possible to solve it analytically [12,15], it is more useful to find approximations in the region of interest, such that we can calculate the rate constants as a function of the different parameters directly. An interesting strategy is to calculate an average Thiele modulus which can be subsequently used in the well-known solutions for the layer mass balance for a normal first-order reaction. This is the average Thiele modulus assumption shown in Figure 1. This approximation is valid when B is low, meaning the irradiance profile in the catalyst layer is almost linear, or when the concentration profile is not very steep, when averaging the reactivity using the average Thiele modulus does not affect the total reaction rate. The accuracy of the model is dependent on the chosen type of averaging. Here, we only discuss the use of the arithmetic mean of the Thiele modulus squared. The validity of the model as a function of B and the Thiele modulus is discussed in the results section. The average Thiele modulus squared as a function of ϕ_0^2 and B is equal to

$$\overline{\phi}^2 = \int_0^1 \phi^2(\tilde{y}) d\tilde{y} = \frac{\phi_0^2}{B}(1 - e^{-B}) \qquad 13$$

The average Thiele modulus can be directly used in the analytical solution of Eq. **Error! Reference source not found.**, which means the equation for calculating the dimensionless molar flux of the photocatalytic process and the conventional catalytic process is formally the same. As a result, the dimensionless molar flux for the photocatalytic process is equal to

$$\tilde{N} = \overline{\phi}\tanh(\overline{\phi}), \quad 14$$

which is an approximation of the exact solution of Eq. **Error! Reference source not found.**. The accuracy of this approximation is compared with the numerical solution of Eq. **Error! Reference source not found.** in the Results section.

A photocatalytic reactor can be kinetically optimized by maximizing the molar flux through the catalyst surface. Here, an important controllable design parameter is the catalyst layer thickness δ. When increasing the catalyst layer thickness the molar flux through the surface increases until all the light energy is absorbed, or until all the species have reacted. However, a problem with using the dimensionless molar flux is that $\overline{\phi}$ keeps on increasing towards infinity as a function of the catalyst layer thickness, which means the dimensionless molar flux $\tilde{N}$ keeps increasing infinitely high values when the catalyst layer thickness increases. This problem is solved by decoupling the dimensionless flux from the catalyst layer thickness by dividing it with B. We can redefine the dimensionless flux as

$$\tilde{N}_m = \frac{1}{B}\tilde{N}, \quad 15$$

where $\tilde{N}_m$ is the modified dimensionless flux. Because both $\overline{\phi}$ and B contain the catalyst layer thickness δ, the modified dimensionless flux will reach a maximum value as a function of the catalyst layer thickness after the tangent hyperbole in Eq. **Error! Reference source not found.**

approaches 1. Also the Thiele modulus can be decoupled from the catalyst layer thickness when rewriting it as a function of B:

$$\phi_m^2 = \frac{1}{B^2}\phi_0^2 = \frac{\alpha_1 (I_0\beta)^{\alpha_2}}{D_e(\alpha_2\beta)^2} \quad 16$$

In the optimization process, the dimensionless molar flux $\tilde{N}_m$ can now be analyzed as a function of two different independent dimensionless groups ϕ_m and B. ϕ_m only contains the material properties and the incident irradiance I_0, a variable which can be easily varied during an experiment while B contains the catalyst layer thickness δ, a design parameter. As a result the effect of the material properties and the incident irradiance can be observed independently from the catalyst layer thickness.

2.4 Reactor mass balance for single-channel and multiple-channel reactors

In Figure 5, a schematic representation of a typical reactor channel is presented. $c_{\text{in}}\ (\text{mol m}^{-3})$ is the inlet concentration, $c_{\text{out}}\ (\text{mol m}^{-3})$ the outlet concentration, $c_s(\text{mol m}^{-3})$ is the concentration at the catalyst surface, and N is the molar flux through the catalyst surface.

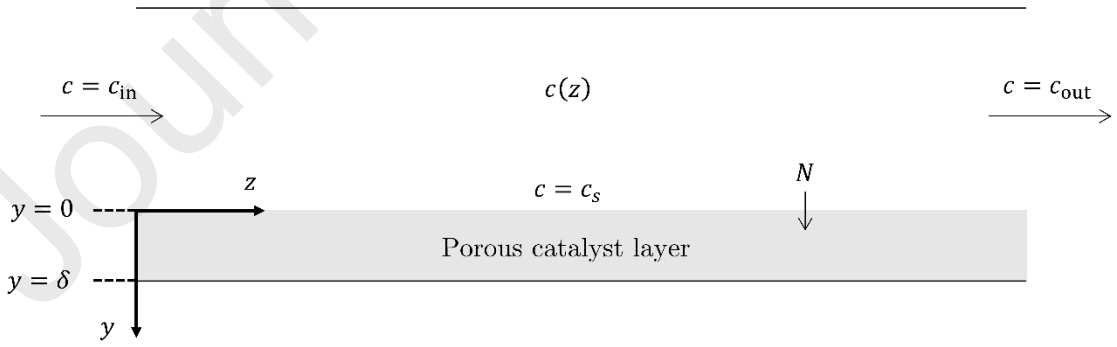

Figure 5: Schematic representation of a reactor channel for which the kinetic parameters are calculated

The mass balance for an individual channel is composed using the CSTR reactor approximation meaning there is no concentration profile in the radial direction and the axial direction. As a result,

the catalyst surface concentration can be assumed equal to the bulk concentration $c(z)$ and the measured outlet concentration is equal to the species concentration in the reactor ($c(z)$) meaning it can be used directly for calculation of the kinetic parameters. Experimentally one can operate in this regime when setting up a differential reactor in loop (conversion per pass < 5%) [11,14,25]. The experimental reaction rate for a first-order reaction assuming constant concentration is equal to

$$R_v = k_{\text{app}} c_{\text{out}}, \tag{17}$$

where R_{v} ($\text{mol m}^{-3}\text{s}^{-1}$) is the reaction rate written in terms of liquid volume, k_{app} (s^{-1}) is the measured apparent first-order rate constant and $c(z)$ (mol m^{-3}) is the species concentration. The model equations are predicting a dimensionless molar flux through the catalyst surface is dependent on the concentration at the catalyst surface. Because of the CSTR approximation made in the reactor channel, the concentration is constant and the molar flux calculated from its dimensionless form is equal to

$$N = \frac{D_e c}{\delta}\tilde{N} = D_e c \alpha_2 \beta \tilde{N}_m, \tag{18}$$

where N ($\text{mol m}^{-2}\text{s}^{-1}$) is the molar flux, $\tilde{N}$ ($-$) is the dimensionless flux calculated using Eq. **Error! Reference source not found.**, and $\tilde{N}_m$ ($-$) is the modified dimensionless flux. As already explained using Figure 2, in a photocatalytic structure the light intensity decays when going radially deeper inside the bed. As a result, the molar flux through the catalytic surface is different in every catalyst layer. Eq. **Error! Reference source not found.** can be applied in every channel separately and averaged to obtain the net result of the reactor. The resulting number is the total molar flux or global reaction rate for that specific reactor setup and is defined as $\overline{N}$. For single-channel reactors with 1 coated layer, the average molar flux $\overline{N}$ is equal to N.

To obtain the apparent first-order rate constant, the rate of disappearance in the liquid must be equal to the rate through the catalyst surface:

$$k_{\mathrm{app}} c V_l = \overline{N} A_s \qquad 19$$

Where V_l (m^3) is the liquid volume, A_s (m^2) is the total surface area, and $\overline{N}$ $(\mathrm{mol\ m^{-2} s^{-1}})$ is the average molar flux. Rearranging the equation yields an expression for k_{app}:

$$k_{\mathrm{app}} = \overline{N} \frac{A_s}{c V_l} \qquad 20$$

In a structure like a packed bed, the channels are interconnected, which means channels where the conversion is larger are likely to underestimate the reaction rate. Therefore, the conversion is required to stay low for the fitting to be accurate.

3 Results

3.1 Single-channel analysis

Before the analysis of a multi-channel reactor, we look at the solutions for a single-channel reactor. Because a cross-current illuminated translucent structured photocatalytic reactor is basically a stack of channels with decaying reactivity over its cross-section, the analysis in this section can be used to clarify the design of a structured reactor later on.

Together with the solutions using the analytical expressions described in the previous section, a graphical method is presented to evaluate the kinetics of a single-channel reactor. In Figure 6, the modified dimensionless flux $\tilde{N}_m$ (Eq. **Error! Reference source not found.**) is plotted as a function of B and ϕ_m^2. This flux is calculated by numerically solving Eq. **Error! Reference source not found.** for different values of B and ϕ_0^2. Note that we specifically plot the results as a function of ϕ_m^2 because it is independent of the catalyst layer thickness δ, a design parameter. The full black

Journal Pre-proofs

contour lines are isoflux lines representing combinations of B and ϕ_m^2 yielding the same modified dimensionless flux ($\tilde{N}_m$). The dashed black line marks the threshold where B is 95 % of the value where the flux becomes independent of B. Increasing the catalyst layer thickness when all light energy is already absorbed, does not increase the reactivity. Hence, the molar flux $\tilde{N}_m$ does no longer change.

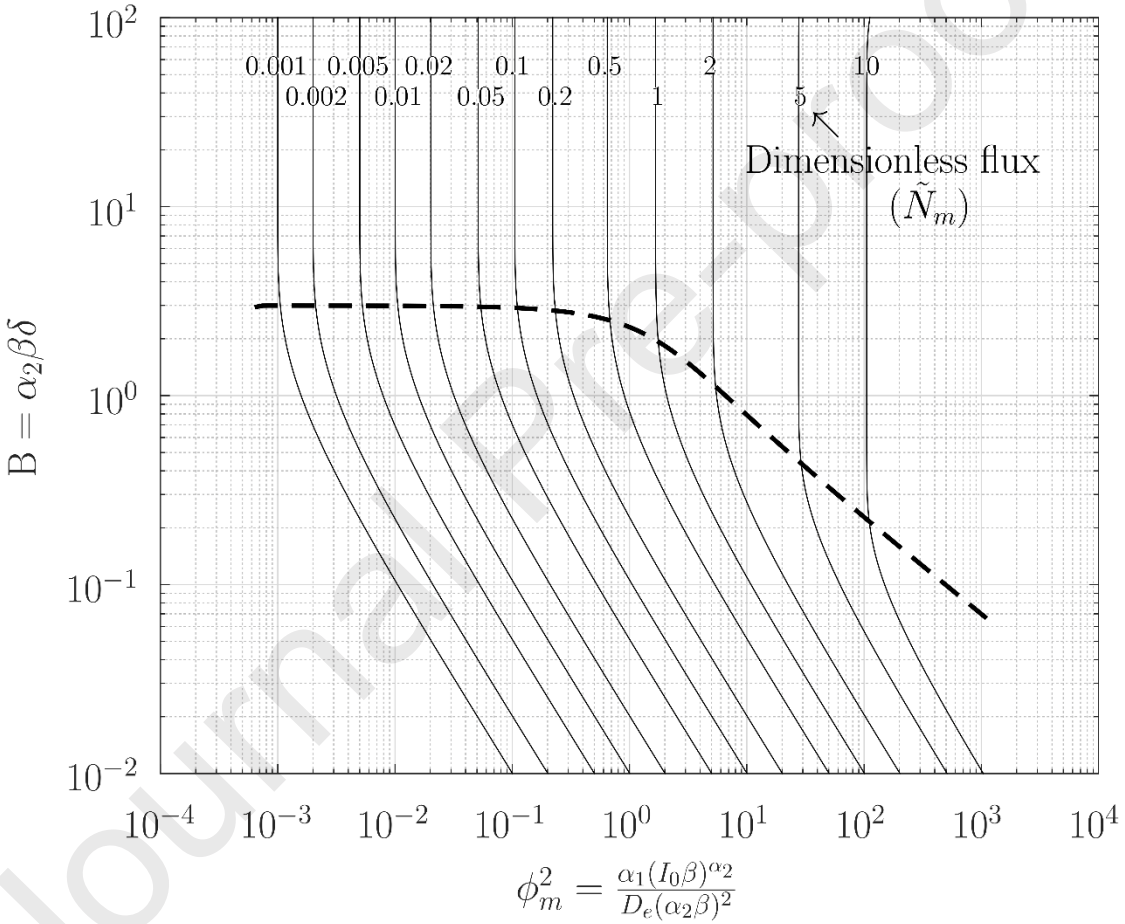

Figure 6: The modified dimensionless flux $\tilde{N}_m$ as a function of ϕ_m^2 and B. The full black contour lines are isoflux lines. For $\tilde{N}_m$, the dashed black line marks the threshold where the flux $\tilde{N}_m$ becomes independent of B.

Suppose a single-channel photocatalytic reactor with a single coated catalyst layer. α_1 and α_2 are determined by the catalytic and chemical system. The physical properties of the catalyst layer determine the effective diffusivity D_e and the absorption coefficient β. Hence, the important

variable is the incoming light intensity I_0. If the light intensity is kept constant, ϕ_m^2 is constant and a straight vertical line can be plotted on the figure to fully characterize the kinetic performance of the layer. When B is low, which implies a thin catalyst, the vertical line crosses multiple isoflux lines when B increases. When B is large, the vertical line becomes parallel with the isoflux lines, meaning that all the light energy is absorbed. The application of this figure on a practical example is demonstrated later.

The graphical method is based on the numerical solution of Eq. **Error! Reference source not found.**. The analytical expressions (Eqs. **Error! Reference source not found.** and **Error! Reference source not found.**) derived in section 2.3 can also be used to calculate the same fluxes. However, these equations are based on approximations and are not accurate for every value of ϕ_m^2 and B. In Figure 7, the ratio of the analytical modified dimensionless flux $\tilde{N}_{m,a}$ to the numerical modified dimensionless flux $\tilde{N}_{m,n}$ is shown for different values of ϕ_m^2 and B.

Journal Pre-proofs

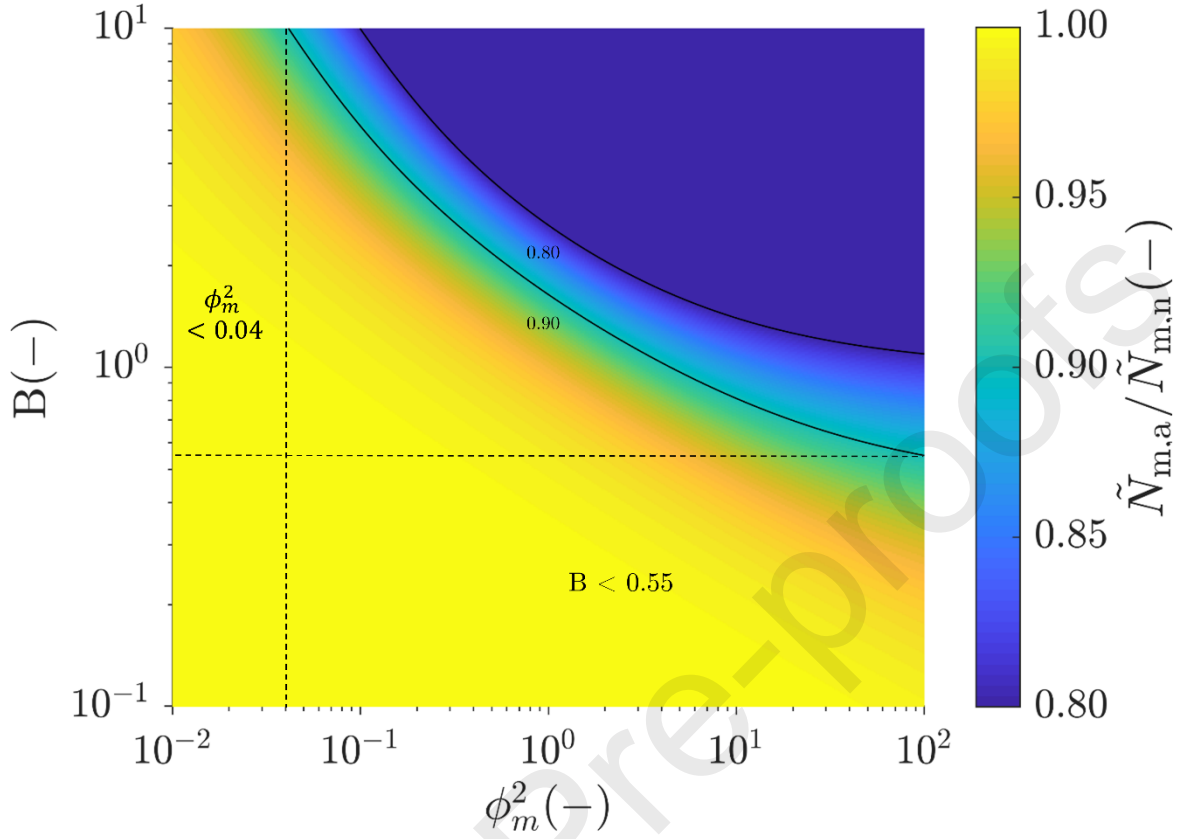

Figure 7: The modified analytically calculated flux $\tilde{N}_{m,a}$ using Eq. **Error! Reference source not found.** and Eq. **Error! Reference source not found.** divided by the numerically obtained flux $\tilde{N}_{m,n}$ for different values of B and ϕ_m^2. The contour lines represent a 10 % and 20 % error margin on the simplified model.

The figure shows three different regimes: A limit where B lower than 0.55, a limit where ϕ_m^2 is smaller than 0.04, and a limit where B as well as ϕ_m^2 are larger. If B is small, then the exponential term in Eq. **Error! Reference source not found.** is nearly equal to 1 and there is almost no drop off the light intensity throughout the catalytic layer. Consequently, as B goes to zero, Eq. **Error! Reference source not found.** increasingly approximates the typical diffusion-reaction equation encountered in non-photocatalytic reactions. As a result, the solution of the equation follows normal first-order behavior and the analytical solution is valid even for larger ϕ_m^2, when the concentration profile is steep due to chemical reaction being much faster than internal transport by diffusion. When ϕ_m^2 is smaller than 0.04, the concentration profile is nearly flat. Here, averaging

the reactivity by using an arithmetic average $\overline{\phi}^2$ is a good approximation because the reagents are well distributed over the complete layer because of fast internal diffusion or slow reaction. When both B and ϕ_m^2 are large, the approximation fails because averaging the reactivity over the layer creates a mismatch between energy absorption and concentration distribution. For example, if all light energy is absorbed in the first parts of the layer and the reagents are only present in this area, then averaging the reactivity over the whole layer thickness will vastly underpredict the reaction rate.

Data from Vezzoli et al. [21] was used to check the validity of using Figure 6 and the analytical equations for predicting the rate constants of a single-channel reactor. The study of Vezzoli varies the coating thickness and reports the apparent reaction rates and conversion while not being limited by external mass transport from the bulk to the catalyst surface. The latter is very important since the reactor model does not take into account bulk mass transport. They also report the effective diffusivity and absorptivity of their catalytic layer which is composed of TiO_2. In Table 1, the relevant experimental data points from their research is presented together with the model predictions. Firstly, the apparent rate constant k_{app} is calculated using the experimentally measured conversions. Secondly, our model is calibrated by calculating B and the modified dimensionless flux ($\tilde{N}_m$) from the apparent first-order rate constants for one experimental point (measurement 1, Table 1). For the calculated rate constants and B the following physical parameters are retrieved from Vezzoli et al.: $D_e = 2.929 \times 10^{-10}\, m^2 s^{-1}$, $\beta = 600\,000\, m^{-1}$, $V_l = 21.56 \times 10^{-6}\, m^3$ and $A_{\mathrm{s}} = 0.02156\, m^2$. Normally, for the calculation of B, $\alpha_2$is required. α_2 is determined varying the light intensity experimentally. If no model predictions as a function of the light intensity are needed or no data is available to determine α_2, it can be arbitrarily taken equal to 1 or extracted from the literature. Knowing $\tilde{N}_m$ and B for one data point we can calculate ϕ_m^2 and α_1 via Eqs. **Error!**

Reference source not found., **Error! Reference source not found.**, **Error! Reference source not found.**, and **Error! Reference source not found.**. The molar flux and the apparent rate constants can now be calculated for different catalyst layer thicknesses. An alternative for the direct calculation from the equations is to graphically determine ϕ_m^2 using Figure 6. In Figure 8, a modified version of Figure 6 is plotted.

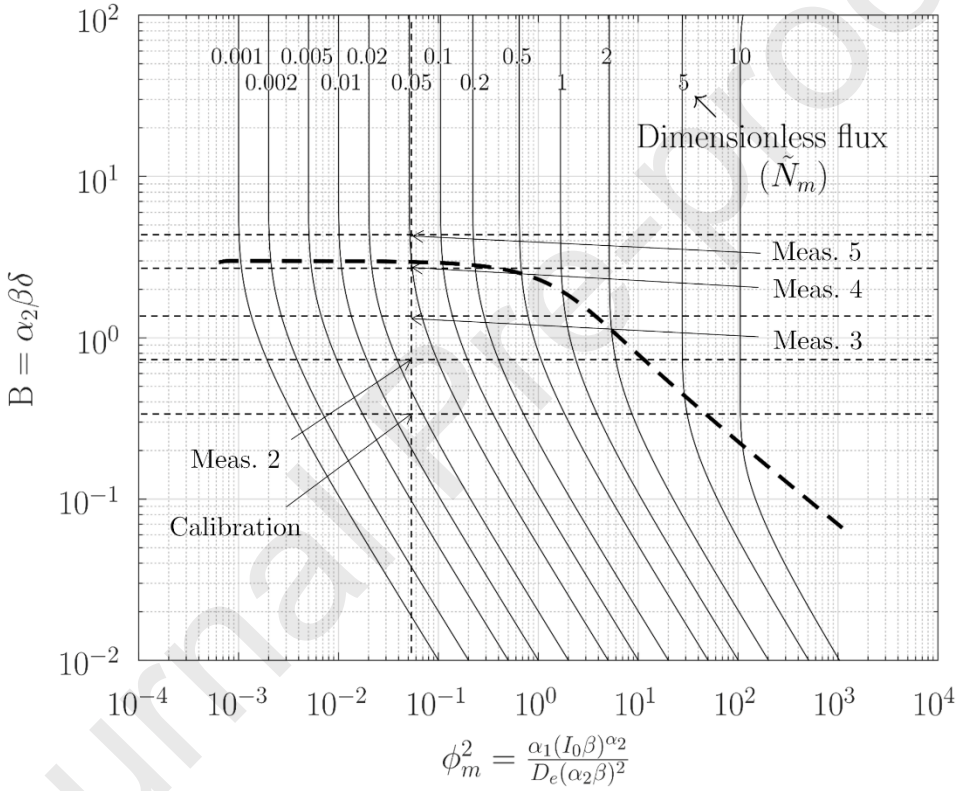

Figure 8: Application of the graphical method on data from Vezzoli et al.

Table 1: Calibration of the model with experimental data from Vezzoli et al. Measurement 1 is used to calibrate the model and to find ϕ_m^2. $k_{\mathrm{app}}\ (\mathrm{s}^{-1})$, $k_{\mathrm{app,\ n}}\ (\mathrm{s}^{-1})$ and $k_{\mathrm{app,\ a}}\ (\mathrm{s}^{-1})$ are respectively the measured, numerically predicted, and analytically predicted rate constants, respectively. $\alpha_1 = 1.3745 \times 10^{-7}((\mathrm{m}^3\,\mathrm{W}^{-1})^{\alpha_2}\mathrm{s}^{-1})$.

Meas.	$\delta\ (\mu m)$	B	$\mathrm{B}^{-1}\tilde{N}$	ϕ_0^2	ϕ_m^2	$k_{\mathrm{app}}\ (\mathrm{s}^{-1})$	$k_{\mathrm{app,n}}\ (\mathrm{s}^{-1})$	$k_{\mathrm{app,a}}\ (\mathrm{s}^{-1})$
1	0.52	0.312	0.0147	0.0054	0.0553	0.00259	0.00258	0.00260
2	1.21	0.726	0.0280	0.0291	0.0553	0.00624	0.00492	0.00498
3	2.24	1.344	0.0404	0.0999	0.0553	0.00765	0.00709	0.00706
4	4.77	2.862	0.0492	0.4529	0.0553	0.00800	0.00865	0.00873

5	7.01	4.206	0.0523	0.9782	0.0553	0.00823	0.00918	0.00890

Again, we require B and $\tilde{N}_m$ from one experiment. Now, if we draw a horizontal line at $B = 0.312$, we identify ϕ_m^2 at the point where $\tilde{N}_m = 0.0147$. Subsequently, a vertical line can be drawn for $\phi_m^2 = 0.0553$. For every catalyst layer thickness the B value changes but ϕ_m^2 stays constant and the intersection between the vertical line and the horizontal lines yields the predicted modified flux. This flux is inserted in Eq. **Error! Reference source not found.** to calculate the rate constants k_{app}.

Figure 9 shows the experimental and predicted values for different catalyst layer thicknesses. The optimal layer thickness δ is reached when the rate constant becomes independent of the catalyst layer thickness. Physically this means all light energy is absorbed, or all reagents are depleted in the inner parts of the layer. Here, based on a visual observation, the minimum layer thickness for optimal performance is equal to 3 μm. The analytical and numerical predictions are in agreement until B or the catalyst layer thickness becomes too large. The same conclusion is made by evaluating the accuracy of the analytical model for the calculated parameters ϕ_m^2 and B in Figure 7. For larger values of B (measurement 5 in Table 1), which is the case for a catalyst layer thickness of 7 µm, the analytical model starts to deviate from the numerical model.

Journal Pre-proofs

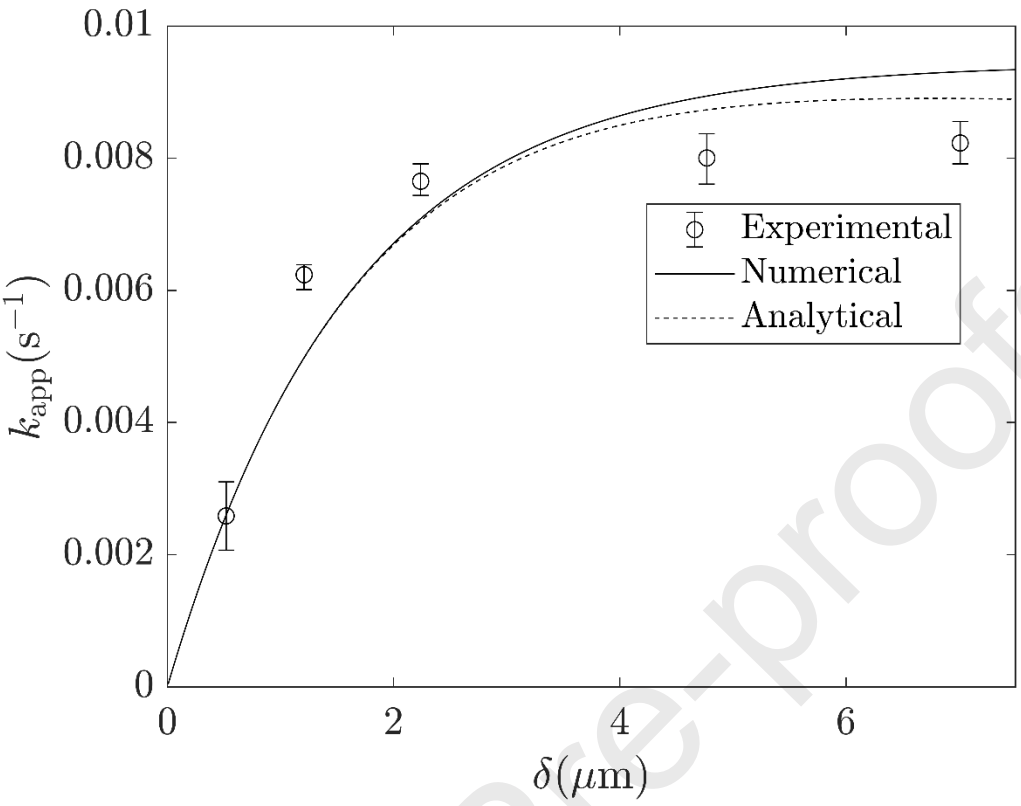

Figure 9: Apparent first-order rate constant as a function of the catalyst layer thickness.

3.2 Multi-channel optimization: numerical vs analytical approach

Front-side illuminated single-channel reactors are optimized by increasing the catalyst layer thickness until the incoming light energy is absorbed. Multi-channel reactors have the possibility to have thinner individual catalyst layers while maintaining the same total catalyst loading as a single-channel device. It allows to cope with possible diffusion limitations inside the catalyst layer. As a result, there will be an optimal combination of layer thickness and number of structural layers. However, adding channels to a structure increases scattering and one has to take into account both front-, and back-side illumination. The solution of the optimization problem can then only be solved numerically. Predicting scattering requires a light model which calculates the forward and backward fluxes, as well as the scattering losses of every channel. With the energy fluxes in the respective channels Eq. **Error! Reference source not found.** can be numerically solved. In

Journal Pre-proofs

contrast, scattering and back-side illumination are neglected for the analytical model (see theory section and Figure 1). Hence, although not entirely valid or accurate, it is assumed that the optimal catalyst layer thickness is not very sensitive to the presence of back-side illumination or scattering because the reactor is being designed such that the optimal point will be found in the region where there are almost no diffusion limitations. In this region the concentration profile is not very steep which means that the actual energy absorption profile along the catalyst layer is less important which means it does not matter from which side the energy is provided.

In the numerical model for multiple channels, the earlier described dimensionless group ϕ_m^2 cannot be defined due to the extra term describing back-side illumination in the reaction rate equation. Consequently, the analytical and numerical models can only be compared for specific cases and not as a function of one dimensionless parameter. Here, we select the irradiance as a parameter to compare the optimization outcome because it is easily adjusted experimentally. The effective diffusivity D_e is often a catalyst layer characteristic which is fixed. In Figure 10, the molar flux as a function of the irradiance is plotted for both models. The more rigorous numerical model is used as a reference to test the validity of the analytical model. The analytical model is calibrated to match the numerical data using α_1.

Journal Pre-proofs

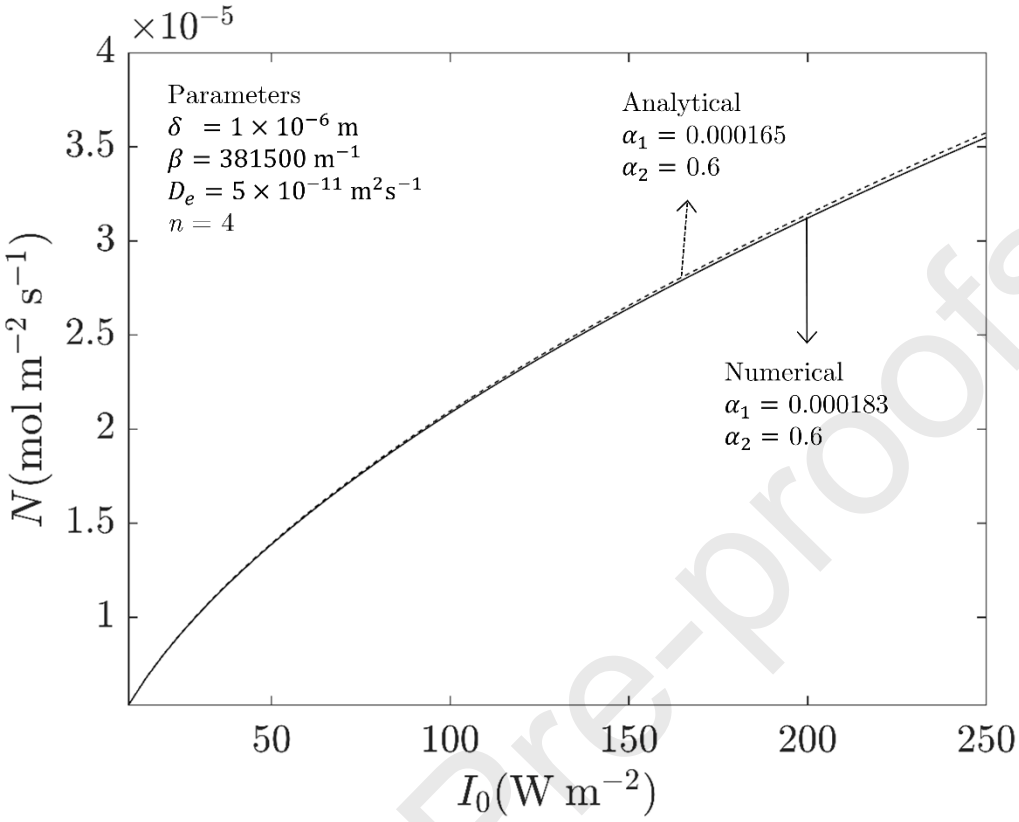

Figure 10: Molar flux through the catalytic surface as a function of the irradiance for the full numerical calculation and the analytical approximation. See Figure 1 for an overview of the different assumptions and models used in this work.

After the calibration step, the models are solved for various combinations of the catalyst layer thickness and the number of layers for different light intensities. Every light intensity gives a dataset of values containing the solution of Eq. **Error! Reference source not found.**, which is the molar flux as a function of the catalyst layer thickness and the number of structural layers. In Figure 11, the relative molar flux (N_{rel}) calculated for $I_0 = 200\ \mathrm{W\ m^{-2}}$ is plotted as a function of the catalyst layer thickness and the number of layers. The relative molar flux (N_{rel}) is equal to the molar flux (N) divided by the maximum molar flux in the dataset (N_{max}). Despite the number of layers being a discrete parameter, it is plotted on a continuous contour plot for ease of visualization.

Journal Pre-proofs

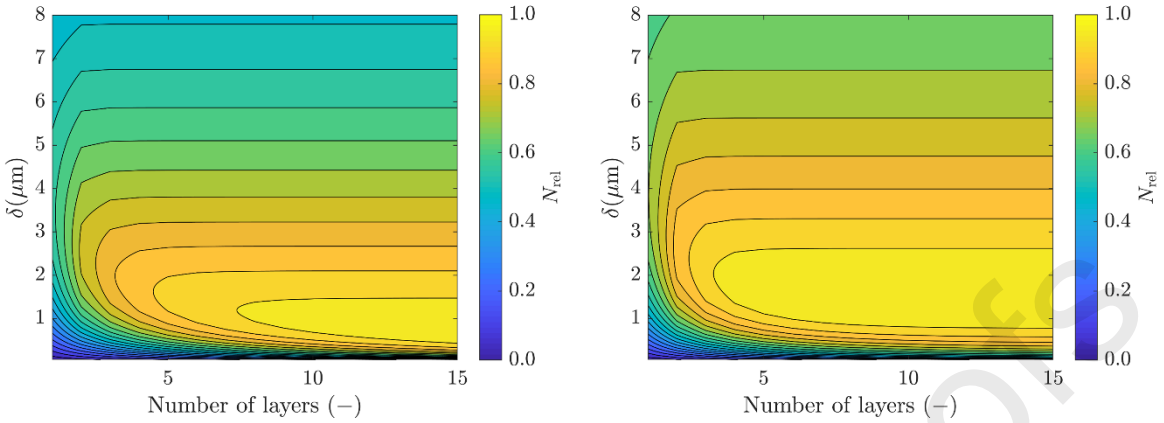

Figure 11: Relative molar flux (N/N_{max}) as a function of the layer thickness δ (µm) and the number of layers for an irradiance of 200 W m^{-2}. The molar flux is standardized for the maximum value in the complete dataset (Left) The analytical solution. (Right) The numerical solution. Contour lines are plotted from 0.01 to 0.95.

In both models, the optimal point is defined by a range of parameters. For example, in the numerical calculation (Right) the brightest yellow area, which represents the area where the relative molar flux is at least equal to 0.95, covers a structural layer number from 3 to 15 and a catalyst layer thickness that can vary from 0.85 µm until 2.65 µm. This means that although there is an optimal working point, the optimal solution to this problem is defined by a region of parameters and it seems that the minimum catalyst layer thickness and number of layers is important. For this reason it is better to define an optimal region instead of a single optimal point. Between the two model outcomes, there are differences. The optimal region of the analytical model is smaller and shifted towards a larger number of layers and thinner catalyst layers in the analytical model. This is because scattering is not being accounted for and because back-side illumination is ignored. Scattering is important for thinner layers, while back-side illumination is important for thicker layers when diffusion limitations become important. As a result, the analytical model has the tendency to under-predict the optimal catalyst layer thickness.

Journal Pre-proofs

The shape and size of the optimal region in Figure 11 varies with the light intensity. If we want to define optimums as a function of the irradiance, we need to choose a proper value from this region for every light intensity. This is done by defining criteria based on minimum catalyst layer thickness and a minimum number of structural layers. To begin with, we can draw a vertical line on Figure 11 at every discrete number of layers and evaluate the flux as a function of the catalyst layer thickness. This way, the optimization problem will reduce from 3 parameter dimensions I_0, δ and n to 2 dimensions I_0 and n. Along the defined vertical line, the relative molar flux first increases relatively sharply before reaching a maximum, to finally move away again as a function of increasing catalyst layer thickness. For every vertical line, which means for every number of layers, we select this maximum relative molar flux value and the two values which are 95 % of the maximum value. In Figure 12, the maximum relative molar flux is plotted as a function of different numbers of structural layers for 200 W m^{-2}. The full black line and dashed black line are pointing to the 95 % and 90 % boundary, respectively.

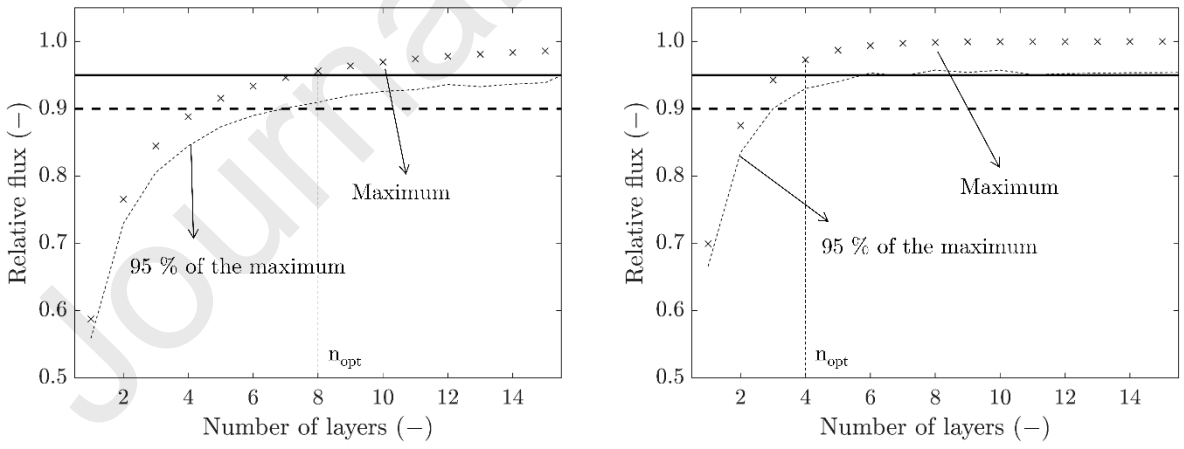

Figure 12: The maximum relative molar flux for a particular number of structural layers for a light intensity of 200 W m^{-2}. The dotted line indicates the 95 % flux interval calculated for a particular number of layers. (Left) The analytical solution. (Right) The numerical solution.

For every value for the number of structural layers, we now have an optimal range of catalyst layer thicknesses. Now, the optimal number of structural layers needs to be selected. From Figure 12, it is concluded that after a steep increase in the maximum value of the relative molar flux a constant value is reached. Additional structural layers will not yield a larger relative molar flux because all the light energy is already consumed. In the analytical model, the plateau is only reached at a larger number of layers because scattering is not accounted for, which promotes the use of more structural layers. A smaller reactor is preferred if it has equal productivity in comparison with the larger reactor. For this reason, we can define the optimal number of layers at the point where the relative molar flux becomes 95 % of the maximum value in the dataset. This is indicated by the horizontal full black line.

Now that the optimization problem is solved for a light intensity of 200 W m^{-2}, we can easily apply this to various light intensities. In Figure 13, the identified optimal catalyst layer thickness region and optimal number of layers n is plotted as a function of the irradiance using two different criteria for the analytical model. In Figure 13A and In Figure 13B, the optimum is identified using 95 % criterion corresponding to the full black line in Figure 12. In Figure 13C and in Figure 13D, the criterion is altered for the analytical model corresponding to the dashed horizontal line on the left side of Figure 12.

Journal Pre-proofs

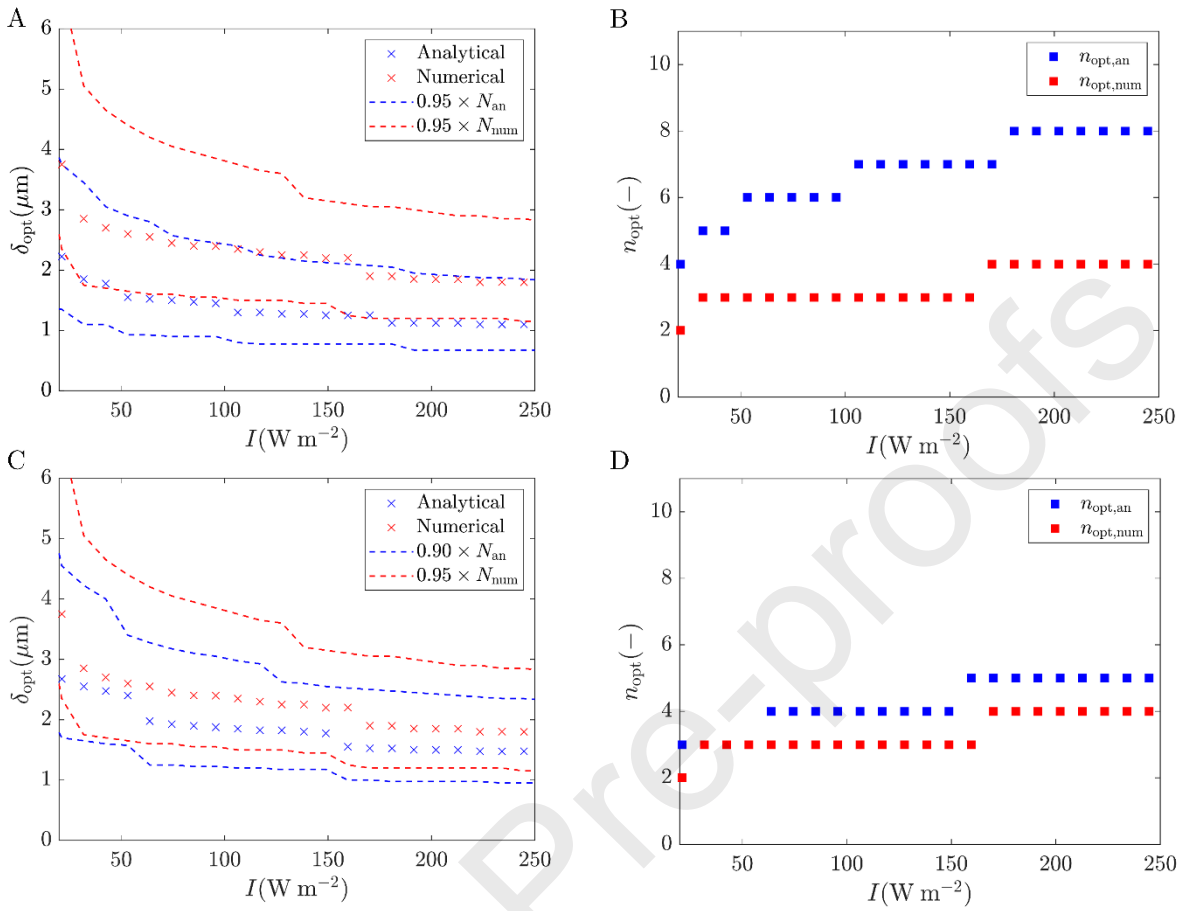

Figure 13: Optimal layer thickness (δ) and optimal number of layers (n_{opt}) as a function of the irradiance (I) for the analytical model (blue) and the numerical model (red). A and B are the optimal values for a confidence interval criterion of 0.95 (full line Figure 12). C and D are the optimal values for a confidence interval criterion for the analytical solution of 0.90 (dashed line on the left side of Figure 12).

When the irradiance increases, the reactivity in the layer increases, and as a result the optimal layer thickness decreases and the optimal number of layers increases. This is expected because a higher reaction rate inside the catalyst layer increases the chance for diffusion limitations. This trend is observed for both models. Corresponding to the results presented in Figure 11, the interval for optimal choice of δ is relatively wide. An important observation is that the lower boundary of the numerical prediction overlaps with the approximate analytical prediction. When using the same criterion for both the analytical and numerical model, the optimal number of layers for the analytical model is much smaller. This is due to the underestimation of scattering in this model

leading to a larger number of layers being more favorable. In Figure 13D, this is addressed by taking a less strict optimization criterion for the analytical model. Taking into account the assumptions it is possible to use the prediction of the analytical model, which is beneficial because the optimal design parameters can be expressed as a function of dimensionless parameters.

Knowing now the differences between the accurate numerical model and the analytical approximation, a more general solution can be presented as a function of the modified Thiele modulus, just like for the single-channel reactor. Since ϕ_m^2 changes in every channel due to varying light intensity, the optimal solution can be displayed as a function of ϕ_m^2 at the illumination inlet of the reactor (the reactor wall). Despite the good prediction of the optimal catalyst layer thickness, the discrepancy between both models and the sensitivity in the optimal region causes an over prediction of the number of layers. A solution is to redefine the criterion for selecting the optimal number of layers. For the analytical model, we choose the number of layers at the point where the relative molar flux becomes 90 % of the maximum value in the dataset. This is indicated by the point where the dashed horizontal line crosses the maximum relative flux values in Figure 12. In Figure 14 the optimal optical density is plotted as a function of parameters B and ϕ_m^2 with ϕ_m^2 evaluated at the illuminated reactor wall. The optimal number of structural layers (n) is indicated by the numbers.

Journal Pre-proofs

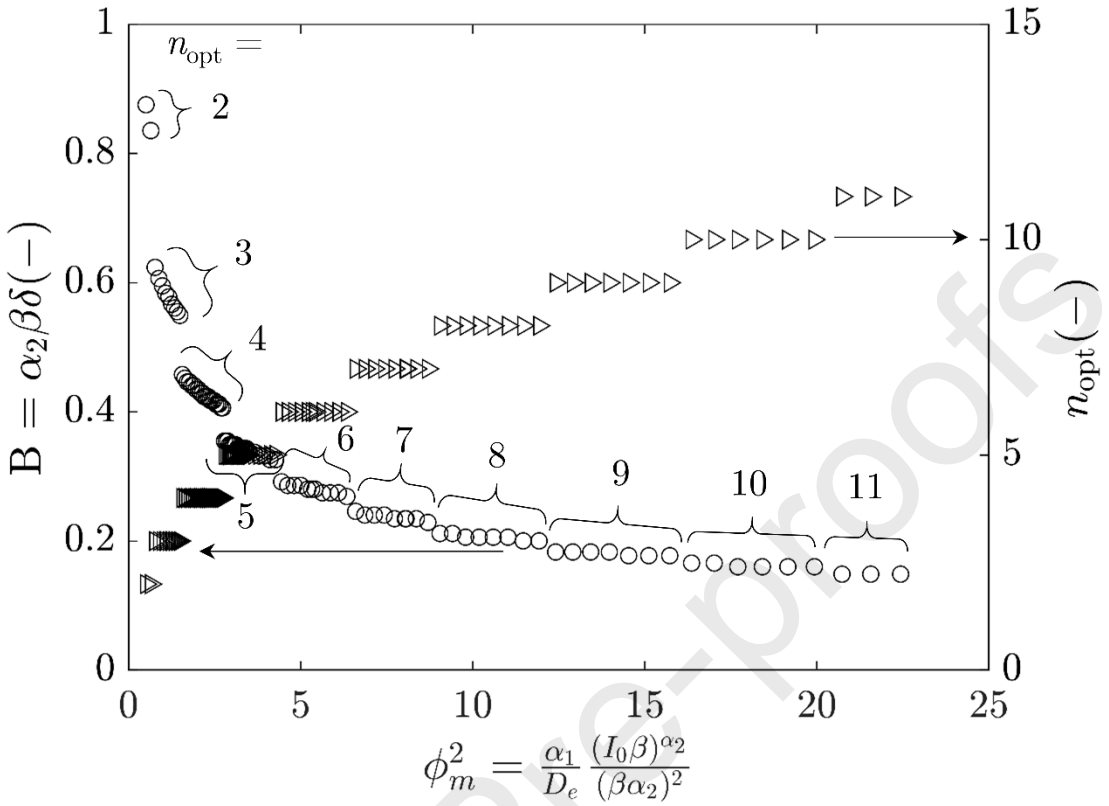

Figure 14: The optimal adjusted optical density B as a function of the reactivity ϕ_m^2. The optimal number of layers is indicated by n.

Increasing ϕ_m^2 increases the reactivity of the layer or increases the diffusion resistance in the catalytic layer. As a result, the optimal B goes down and the optimal number of layers increases. As explained for the numerical method, whenever a new structural layer is added, the optimal B value drops. This is because the number of layers is a discrete parameter. ϕ_m^2 can be directly influenced by changing the irradiance and indirectly by the fitting parameters and the effective diffusivity. The fitting parameters and effective diffusivity are most often properties of the chemical and catalytic system and difficult to influence directly. With this graph, researchers can make a prediction of the optimal catalyst distribution in a structured photocatalytic. Knowing the optimal structural parameters as a function of dimensionless groups is very valuable since the

optimal properties can now be calculated for every fitting parameter, irradiance or effective diffusivity.

3.3 Enhancing the single-channel performance

Looking at the optimal configurations in Figure 14, it is clear that the benefit of multi-channel reactors over a single-channel reactor is dependent on the occurrence of diffusion limitations in the catalyst layer. It was shown that increasing ϕ_m^2, implying an increase in reactivity, decreases the optimal optical thickness $\beta\delta$ and increases the number of optimal layers n_{opt}. In Figure 15, the molar flux of the optimal configuration identified in the previous section is compared with a single-channel reactor with equal catalyst loading. Two discontinuities are identified at $I = 20\ \text{W m}^{-2}$ and $I = 160\ \text{W m}^{-2}$ due to the change in the number of optimal layers for the multi-channeled reactor (see also Figure 15).

Journal Pre-proofs

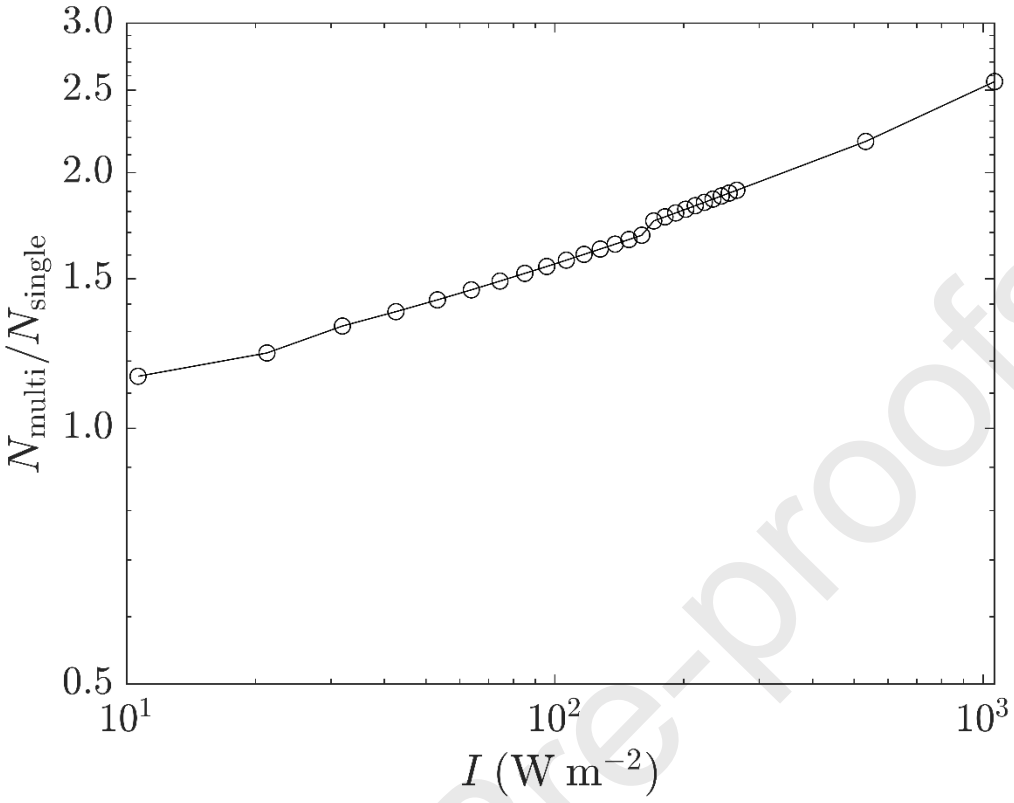

Figure 15: Ratio of the molar flux of a multi-channel reactor and the molar flux of a single-channel reactor for a variable incident irradiance. $D_e = 5 \times 10^{-11}\ \mathrm{m^2 s^{-1}}$, $\beta = 381500\ \mathrm{m^{-1}}$, $\alpha_1 = 0.000183$, $\alpha_2 = 0.6$.

It is always more beneficial to use multi-channel reactors over single-channel reactors, and this benefit becomes increasingly greater for high light intensity. A lower effective diffusivity implies a higher chance for internal mass transfer resistance which also favors the use of multi-channel reactors. For an irradiance lower than 30 W $\mathrm{m^{-2}}$, the performance of the reactor increases with a maximum of 20 %. For an irradiance of 1000 W $\mathrm{m^{-2}}$, the performance more than doubles using a multi-channel reactor. The kinetic improvement can also vary as a function of the different fitting parameters or absorption coefficient. By assessing optimal behavior as a function of dimensionless numbers, all the parameters are accounted for simultaneously. Using the approach described in the previous section, the advantage of a multi-channel reactor can be calculated for a particular case.

4 Conclusions

Models are valuable to predict the behavior of photocatalytic reactors. Often, more complex numerical models are used for specific reactor setups. Although sometimes less accurate, easily useable approximations of these equations are interesting since they give information about a reactor setup for more general problems.

In this work, we present an analytical model and a graphical method which allow for the calculation of the rate constant of a single and multi-channel reactor. It was shown that for a large set of parameters, the analytical approximation provided a very good solution to the problem. In many cases, a photocatalytic reactor is operated in the parameter area where the analytical approximation is accurate. Furthermore, an analysis was performed of a multi-channel reactor using both a numerical model and the analytical approximation. The numerical model was compared with the analytical approach, and it was concluded that the analytical model matches the more elaborate numerical model quite well. This way, the optimal configuration of a cross-current illuminated photocatalytic reactor could be described as a function of dimensionless groups. These strategies help researchers designing optimal catalytic reactors for specific type of catalysts.

Acknowledgments

M. Enis Leblebici acknowledges FWO postdoctoral fellowship.

Nomenclature

Abbreviations

TFM	Two-flux model
SFM	Six-flux model
FSI	Front-side illumination
BSI	Back-side illumination

Symbols

$A_s(m^2)$	Total catalyst surface area
B	Optical thickness modified with α_2
$c\ (\mathrm{mol\ m^{-3}})$	Species concentration
$c_{\mathrm{in}}\ (\mathrm{mol\ m^{-3}})$	Species inlet concentration
$c_{\mathrm{out}}\ (\mathrm{mol\ m^{-3}})$	Species outlet concentration
$c_{\mathrm{s}}\ (\mathrm{mol\ m^{-3}})$	Species concentration at the catalyst surface
$\tilde{c}\ (-)$	Dimensionless species concentration
$D_e(\mathrm{m^2 s^{-1}})$	Effective diffusivity
$E_a(\mathrm{W\ m^{-3}})$	Local rate of energy absorption
$E_f\ (\mathrm{W\ m^{-3}})$	Estimated local volumetric rate of energy absorption only taking in to account the forward photon flux
$E_{f,s}\ (\mathrm{W\ m^{-3}})$	Estimated local volumetric rate of energy absorption only taking in to account the forward photon flux, where the forward photon flux is calculated taking into account scattering.
$E_{\mathrm{max}}\ (\mathrm{W\ m^{-3}})$	Estimated local volumetric rate of energy absorption taking into account forward and backward photon flux
H (m)	Channel height
$I\ (\mathrm{W\ m^{-2}})$	Photon flux or light intensity
$I_f\ (\mathrm{W\ m^{-2}})$	Forward photon flux in a cross-current illuminated reactor
$I_b\ (\mathrm{W\ m^{-2}})$	Backward photon flux in a cross-current illuminated reactor
$I_0\ (\mathrm{W\ m^{-2}})$	Incident photon flux on the catalytic layer
$I_{\mathrm{FSI}}(\mathrm{W\ m^{-2}})$	Front-side incoming light flux
$I_{\mathrm{BSI}}(\mathrm{W\ m^{-2}})$	Back-side incoming light flux
$k_{\mathrm{app}}(s^{-1})$	Apparent first order rate constant
$k_{\mathrm{app,n}}(s^{-1})$	Apparent first order rate constant calculated numerically
$k_{\mathrm{app,a}}(s^{-1})$	Apparent first order rate constant calculated analytically
$k_i\ (\mathrm{s^{-1}})$	Intrinsic first order rate constant
$n\ (-)$	Number of structural layers
$N\ (\mathrm{mol\ m^{-2} s^{-1}})$	Molar flux
$N_{\mathrm{an}}\ (\mathrm{mol\ m^{-2} s^{-1}})$	Analytically calculated molar flux
$N_{\mathrm{num}}\ (\mathrm{mol\ m^{-2} s^{-1}})$	Numerically calculated molar flux
$\tilde{N}(-)$	Dimensionless molar flux
$\tilde{N}_m(-)$	Modified dimensionless molar flux
$N_{\mathrm{max}}\ (-)$	Maximum molar flux in a solution space
$\tilde{N}_{\mathrm{m,a}}(-)$	Modified molar flux calculated using the analytical model
$\tilde{N}_{\mathrm{m,n}}(-)$	Modified molar flux calculated using the numerical model
$N_{\mathrm{rel}}\ (-)$	Relative molar flux defined as the molar flux divided by the maximum molar flux in a solution space.
$Q\ (\mathrm{m^3 s^{-1}})$	Volumetric flow rate
$R_{\mathrm{v}}\ (\mathrm{mol\ m^{-3} s^{-1}})$	Reaction rate written in terms of the liquid volume

$V_l\,(\mathrm{m}^3)$	Liquid reactor volume
$y\,(\mathrm{m})$	Spatial coordinate
$\tilde{y}\,(-)$	Dimensionless spatial coordinate

Greek symbols

α_1	Empirically fitted constant
α_2	Empirically fitted constant between 0 and 1 related to the electron-hole recombination rate
$\beta\,(\mathrm{m}^{-1})$	Absorption coefficient
$\delta\,(\mathrm{m})$	Catalyst layer thickness
$\phi\,(-)$	Thiele modulus
$\phi_0\,(-)$	Maximum Thiele modulus at the catalyst-liquid interphase
$\overline{\phi}\,(-)$	Thiele modulus in the catalyst layer
$\phi_m\,(-)$	Modified Thiele modulus independent of the catalyst layer thickness

5 Bibliography

[1] M.B. Plutschack, B. Pieber, K. Gilmore, P.H. Seeberger, The Hitchhiker's Guide to Flow Chemistry, Chem. Rev. 117 (2017) 11796–11893. doi:10.1021/acs.chemrev.7b00183.

[2] N. Padoin, C. Soares, An explicit correlation for optimal TiO2 film thickness in immobilized photocatalytic reaction systems, Chem. Eng. J. 310 (2017) 381–388. doi:10.1016/j.cej.2016.06.013.

[3] T. Van Gerven, G. Mul, J. Moulijn, A. Stankiewicz, A review of intensification of photocatalytic processes, Chem. Eng. Process. Process Intensif. 46 (2007) 781–789. doi:10.1016/j.cep.2007.05.012.

[4] A. Potdar, L.N. Protasova, L. Thomassen, S. Kuhn, Designed porous milli-scale reactors with enhanced interfacial mass transfer in two-phase flows, React. Chem. Eng. 2 (2017) 137–148. doi:10.1039/c6re00185h.

[5] L. Kiwi-Minsker, A. Renken, Microstructured reactors for catalytic reactions, Catal.

Journal Pre-proofs

Today. 110 (2005) 2–14. doi:10.1016/j.cattod.2005.09.011.

[6] S.W. Verbruggen, S. Ribbens, T. Tytgat, B. Hauchecorne, M. Smits, V. Meynen, P. Cool, J.A. Martens, S. Lenaerts, The benefit of glass bead supports for efficient gas phase photocatalysis: Case study of a commercial and a synthesised photocatalyst, Chem. Eng. J. 174 (2011) 318–325. doi:10.1016/j.cej.2011.09.038.

[7] V. Vaiano, O. Sacco, D. Pisano, D. Sannino, P. Ciambelli, From the design to the development of a continuous fixed bed photoreactor for photocatalytic degradation of organic pollutants in wastewater, Chem. Eng. Sci. 137 (2015) 152–160. doi:10.1016/j.ces.2015.06.023.

[8] A.N. Kouamé, R. Masson, D. Robert, N. Keller, V. Keller, β-SiC foams as a promising structured photocatalytic support for water and air detoxification, Catal. Today. 209 (2013) 13–20. doi:10.1016/j.cattod.2012.12.008.

[9] F. Denny, J. Scott, G.D. Peng, R. Amal, Channelled optical fibre photoreactor for improved air quality control, Chem. Eng. Sci. 65 (2010) 882–889. doi:10.1016/j.ces.2009.09.038.

[10] G. Vella, G.E. Imoberdorf, A. Sclafani, A.E. Cassano, O.M. Alfano, L. Rizzuti, Modeling of a TiO2-coated quartz wool packed bed photocatalytic reactor, Appl. Catal. B Environ. 96 (2010) 399–407. doi:10.1016/j.apcatb.2010.02.037.

[11] T. Claes, A. Dilissen, M.E. Leblebici, T. Van Gerven, Translucent packed bed structures for high throughput photocatalytic reactors, Chem. Eng. J. 361 (2019) 725–735. doi:10.1016/j.cej.2018.12.107.

[12] A. Visan, D. Rafieian, W. Ogieglo, R.G.H. Lammertink, Modeling intrinsic kinetics in

Journal Pre-proofs

immobilized photocatalytic microreactors, Appl. Catal. B Environ. 150–151 (2014) 93–100. doi:10.1016/j.apcatb.2013.12.003.

[13] A.E. Cassano, O.M. Alfano, Reaction engineering of suspended solid heterogeneous photocatalytic reactors, Catal. Today. 58 (2000) 167–197. doi:10.1016/S0920-5861(00)00251-0.

[14] M.E. Leblebici, J. Rongé, J.A. Martens, G.D. Stefanidis, T. Van Gerven, Computational modelling of a photocatalytic UV-LED reactor with internal mass and photon transfer consideration, Chem. Eng. J. 264 (2014) 962–970. doi:10.1016/j.cej.2014.12.013.

[15] M.G. Nielsen, S. Il In, P.C.K. Vesborg, T. Pedersen, K.P. Almtoft, I.H. Andersen, O. Hansen, I. Chorkendorff, A generic model for photocatalytic activity as a function of catalyst thickness, J. Catal. 289 (2012) 62–72. doi:10.1016/j.jcat.2012.01.015.

[16] G. Li Puma, A. Brucato, Dimensionless analysis of slurry photocatalytic reactors using two-flux and six-flux radiation absorption-scattering models, Catal. Today. 122 (2007) 78–90. doi:10.1016/j.cattod.2007.01.027.

[17] A. Brucato, A.E. Cassano, F. Grisafi, G. Montante, L. Rizzuti, G. Vella, Estimating radiant fields in flat heterogeneous photoreactors by the six-flux model, AIChE J. 52 (2006) 3882–3890. doi:10.1002/aic.10984.

[18] G.E. Imoberdorf, A.E. Cassano, H.A. Irazoqui, O.M. Alfano, Simulation of a multi-annular photocatalytic reactor for degradation of perchloroethylene in air: Parametric analysis of radiative energy efficiencies, Chem. Eng. Sci. 62 (2007) 1138–1154. doi:10.1016/j.ces.2006.10.024.

[19] F. Khodadadian, M.W. de Boer, A. Poursaeidesfahani, J.R. van Ommen, A.I. Stankiewicz,

Journal Pre-proofs

R. Lakerveld, Design, characterization and model validation of a LED-based photocatalytic reactor for gas phase applications, Chem. Eng. J. 333 (2018) 456–466. doi:10.1016/j.cej.2017.09.108.

[20] F. Khodadadian, A. Poursaeidesfahani, Z. Li, J.R. van Ommen, A.I. Stankiewicz, R. Lakerveld, Model-Based Optimization of a Photocatalytic Reactor with Light-Emitting Diodes, Chem. Eng. Technol. 39 (2016) 1946–1954. doi:10.1002/ceat.201600010.

[21] M. Vezzoli, T. Farrell, A. Baker, S. Psaltis, W.N. Martens, J.M. Bell, Optimal catalyst thickness in titanium dioxide fixed film reactors: Mathematical modelling and experimental validation, Chem. Eng. J. 234 (2013) 57–65. doi:10.1016/j.cej.2013.08.049.

[22] T. Claes, T. Van Gerven, M.E. Leblebici, Design considerations for photocatalytic structured packed bed reactors, Chem. Eng. J. 403 (2021) 126355. doi:10.1016/j.cej.2020.126355.

[23] J.M. Herrmann, Heterogeneous photocatalysis: Fundamentals and applications to the removal of various types of aqueous pollutants, Catal. Today. 53 (1999) 115–129. doi:10.1016/S0920-5861(99)00107-8.

[24] O. Levenspiel, Chemical Reaction Engineering, 1964. doi:10.1016/0009-2509(64)85017-X.

[25] M. Vezzoli, W.N. Martens, J.M. Bell, Investigation of phenol degradation: True reaction kinetics on fixed film titanium dioxide photocatalyst, Appl. Catal. A Gen. 404 (2011) 155–163. doi:10.1016/j.apcata.2011.07.025.

- Photon and mass transfer in photocatalytic layers were investigated.
- Both single-and multi-channeled (structured) reactors were considered.
- A graphical tool was developed for the determination of catalyst layer kinetics.
- An Analytical model was derived to calculate the optimal catalyst configuration.
- The use of dimensionless groups makes the model generally applicable.

Journal Pre-proofs